HTML ABSTRACT + LINKS

Analysis of the magnetic anisotropy induced by applying a magnetic field during the quenching process in amorphous ribbons

M. Tejedor, J. A. García, J. Carrizo, L. Elbaile,[a] and J. D. Santos
Departamento de Física, Universidad de Oviedo, Calvo Sotelo s/n, 33007 Oviedo, Spain

J. Mira and J. Rivas
Departamento de Física Aplicada, Universidade de Santiago de Compostela, 15706 Santiago de Compostela, Spain

(Received 6 January 2004; accepted 3 August 2004)

The magnetic anisotropy induced in amorphous magnetic ribbons by applying a magnetic field to the melt during the solidification process is analyzed. Using a model based on the magnetization curve and on the evolution of the uniaxial torque with the applied magnetic field, the volume fractions of the sample affected by the different magnetic anisotropies are obtained for the ribbons of composition $Fe_{80}B_{20}$ and $Co_{70}Mn_5Fe_1Mo_1Si_{14}B_9$. The results are compared with those obtained in the ribbons of the same composition but with anisotropies induced by the static magnetic annealing. From these results, the different sources of the field-quenching-induced magnetic anisotropy in those amorphous magnetic ribbons are analyzed. © *2004 American Institute of Physics*. [DOI: 10.1063/1.1798402]

I. INTRODUCTION

Magnetic anisotropy is one of the most important parameters in classifying magnetic materials for different technical applications. In the case of the amorphous magnetic ribbons, different sources during the manufacturing process give rise to the magnetic anisotropy in and out of the plane of the ribbons.[1–3] In some applications of these materials, it is necessary to remove these anisotropies, but there are other applications in which it is necessary to induce the magnetic anisotropies in different directions. One particular case of great importance for the applications of amorphous magnetic ribbons in the magnetostrictive transducers[4] is the induction of the magnetic anisotropy transverse to the ribbon length. Traditionally, the induction of the magnetic anisotropy in amorphous ribbons has been performed by the magnetic-field annealing,[5–7] but recently, the authors have induced a transverse magnetic anisotropy in the amorphous magnetic ribbons by applying a magnetic field during the solidification of the melt.[8] This method has a great advantage that maintains the good mechanical properties of these materials in the as-quenched state.

The study of the magnetic anisotropy sources is important because the control of the magnetic anisotropy will allow us to tailor the amorphous materials to meet the specific technical requirements.

In this work, we present a study of the anisotropy induced by the field-quenching technique developed by the authors in the high Curie temperature and $Fe_{80}B_{20}$ and $Co_{70}Mn_5Fe_1Mo_1Si_{14}B_9$ amorphous ribbons. The evolution of the uniaxial torque and of the magnetization with the applied magnetic field allow us to discriminate the different sources of the induced anisotropy using a model developed by Tejedor *et al.*[9]

[a]Electronic mail: elbaile@pinon.ccu.uniovi.es

II. EXPERIMENTAL PROCEDURE

The ribbons used in this work, of compositions $Fe_{80}B_{20}$ and $Co_{70}Mn_5Fe_1Mo_1Si_{14}B_9$, both with high Curie temperatures of 647 and 623 K, respectively, were made by the quenching technique in our laboratory. One set of ribbons of each composition was made by applying a magnetic field of 0.07 T, transverse to the ribbon during the solidification of the melt on the rotating wheel, and another set was made without the applied magnetic field. The device used to apply the magnetic field has been described elsewhere.[8] Ribbons of 5-mm width and 25-μm thickness were obtained in this way. The amorphicity of the ribbons and the ductility were tested by x-ray diffraction and by creasing test, respectively.

The magnetic-field annealing of the samples made without an applied magnetic field was performed at 520 K in a furnace with an inert Ar atmosphere and with an applied magnetic field of 0.009 T.

The magnetization curves were measured using a vibrating sample magnetometer model DMS-1660 from the Digital Measurements Systems. The torque measurements were performed by means of a high-sensitivity torque magnetometer developed in our laboratory.[10]

In order to avoid shape effects, nearly perfect circular samples were cut out from the ribbons using a method developed in our laboratory.[11] We cut the discs from different parts of the same ribbon and from different ribbons made under the same conditions to be sure that the results were reproducible. The samples were 4 mm in diameter, which is less than the width of the as-prepared ribbon to avoid the effect of the edges. The magnetization was measured on the same disc samples used for the torque measurements.

III. RESULTS AND DISCUSSION

The magnetization curves for all the samples saturated in low fields when measured both in the easy and hard direc-

0021-8979/2004/96(10)/5658/5/$22.00 © 2004 American Institute of Physics

Downloaded 29 Dec 2004 to 193.144.85.71. Redistribution subject to AIP license or copyright, see http://jap.aip.org/jap/copyright.jsp

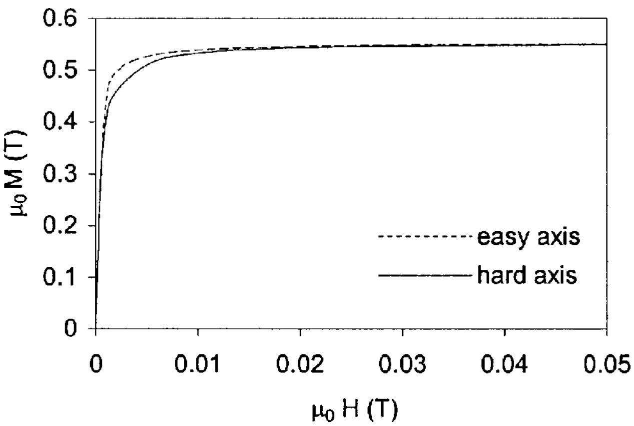

FIG. 1. Evolution of the magnetization with the applied magnetic field for $Co_{70}Mn_5Fe_1Mo_1Si_{14}B_9$, cast with the applied magnetic field.

tions. Figure 1 shows the evolution of magnetization with the applied magnetic field μ_0H for $Co_{70}Mn_5Fe_1Mo_1Si_{14}B_9$ solidified in an applied magnetic field. The other samples had the same behavior. The area enclosed by the two magnetization curves at these low-applied magnetic fields was estimated as 227 Jm^{-3}.

The torque curves of the samples of both compositions made with and without an applied magnetic field have the twofold shape that corresponds to a uniaxial magnetic anisotropy. The samples of $Fe_{80}B_{20}$ obtained without an applied magnetic field have a magnetic anisotropy of $K_u=375$ Jm^{-3}, with the easy axis directed on an average of about 70° away from the ribbon axis. For the samples made with the applied magnetic field, the anisotropy is $K_u=750$ Jm^{-3}, with the easy axis in the transverse direction of the ribbon. In the case of the samples of $Co_{70}Si_{14}B_9Mn_5Fe_1Mo_1$, the results were $K_u=100$ Jm^{-3}, with the easy axis in the longitudinal direction of the ribbon for the samples made without the applied magnetic field, and $K_u=740$ Jm^{-3}, with the easy axis in the transverse direction of the ribbon in the samples made with the applied magnetic field.[8]

Figures 2 and 3 show the evolution of the magnetic anisotropy constant with the applied magnetic field μ_0H for $Fe_{80}B_{20}$ and $Co_{70}Si_{14}B_9Mn_5Fe_1Mo_1$.

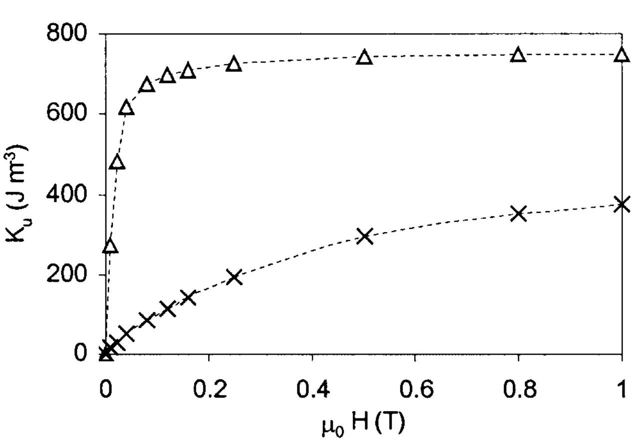

FIG. 2. Evolution of the magnetic anisotropy K_u with the applied magnetic field for $Fe_{80}B_{20}$, cast with (△) and without (×) the applied magnetic field.

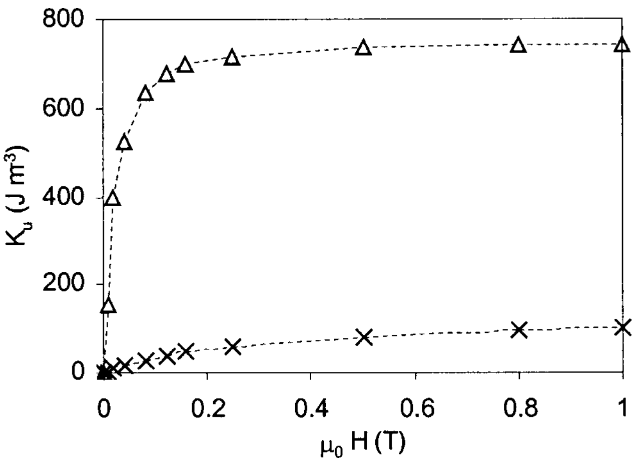

FIG. 3. Evolution of the magnetic anisotropy K_u with the applied magnetic field for $Co_{70}Mn_5Fe_1Mo_1Si_{14}B_9$, cast with (△) and without (×) the applied magnetic field.

The behavior of these curves can be summarized as follows:

(1) For the $Fe_{80}B_{20}$ made without the applied magnetic field, K_u increases slowly and it reaches its maximum value of 375 Jm^{-3} at 0.9 T. For the ribbons of the same composition made with the applied magnetic field, K_u increases rapidly at low fields. At about 0.05 T, the curve bends forming a knee, then increases slowly and practically saturates at 0.5 T. At this magnetic field, the torque per unit volume is 750 Jm^{-3}.

(2) For the $Co_{70}Si_{14}B_9Mn_5Fe_1Mo_1$ ribbons quenched without the applied magnetic field, K_u increases slowly and reaches its maximum value of 100 Jm^{-3} at 0.8 T. For the ribbons made with the applied magnetic field, K_u increases rapidly at low fields. At about 0.1 T, the curve bends form a knee. The curve saturates at about 0.5 T and the maximum value of K_u reached is 740 Jm^{-3}.

The fact that the higher fields were required to saturate the anisotropy torque than to saturate the magnetization was remarked by Tasarov[12] and Kouvel and Graham[13] for the silicon-iron single-crystal discs. These latter authors observed that the effective value of K', deduced from the torque peaks, depended on the applied magnetic field H as

$$K' = K\left(1 - \frac{C}{\sqrt{H}}\right), \tag{1}$$

where K is the real value of the anisotropy constant. They observed that the constant C decreases when the thickness-to-diameter ratio of the disk specimen decreases. This result was attributed to a lack of saturation at the edges of the discs. In our case, the field dependence of K' does not follow the relation (1) and, in addition, there is no appreciable change of the field dependence of the anisotropy constant when the thickness-to-diameter ratio varies.

The area enclosed by the two magnetization curves for $Co_{70}Si_{14}B_9Mn_5Fe_1Mo_1$, solidified in an applied magnetic field, is a good approximation of the uniaxial anisotropy present in the plane of the sample. Then, the value of 227 Jm^{-3} calculated approximately from the area enclosed

Downloaded 29 Dec 2004 to 193.144.85.71. Redistribution subject to AIP license or copyright, see http://jap.aip.org/jap/copyright.jsp

TABLE I. Anisotropy distribution of $Fe_{80}B_{20}$ in the samples made with and without the applied magnetic field.

		Without the applied magnetic field			With the applied magnetic field		
$\mu_0 H$ (*T*)	K_i (Jm^{-3})	T_u (Jm^{-3})	$f_i(10^{-2})$	$f_i K_i$	T_u (Jm^{-3})	$f_i(10^{-2})$	$f_i K_i$
0.9947	633275	375	0.006	39.8	750	0.000	0.00
0.7947	505951	367	0.030	153	750	0.002	10.6
0.4947	314965	297	0.028	88.4	746	0.010	33.0
0.2447	155810	194	0.026	40.6	726	0.014	21.2
0.1547	98514	142	0.023	22.8	711	0.021	20.6
0.1147	73049	113	0.004	2.87	699	0.039	28.7
0.0747	47585	83	0.016	7.47	677	0.110	52.3
0.0347	22120	49	0.008	1.74	627	0.958	212
0.0147	9387	31	0.079	7.37	480	2.081	195
0.0047	3021	17	0.220	6.64	274	5.834	176

by the magnetization curves at low fields could be related to the contribution to the anisotropy due to the zones in the sample exhibiting low anisotropy fields.

To analyze the in-plane magnetic anisotropy in the amorphous ribbons obtained by the torque magnetometry, we have applied a method developed by Tejedor *et al.*[9] to the mentioned results. In this method, it is assumed that the sample is formed by an indefinite number of regions that occupy different volume fractions and exhibit different magnetic anisotropies. We suppose that these regions are the small defects (microholes, crystalline precipitates, composition fluctuations, overstrained zones, etc.) in the amorphous matrix frozen-in during the quenching process. These defects can exhibit a large magnetic anisotropy along any direction, but mainly along the ribbon axis due to the manufacturing process (oriented internal strains, deformed prolated microholes, etc.). These regions occupy a very small volume fraction, and the interaction between them can be ignored. In each region, the uniaxial torque amplitude varies linearly with the applied field. The uniaxial torque per unit volume T_i of the ith region increases linearly until the anisotropy field H_i is reached. Then, the uniaxial torque amplitude T_i reaches a maximum value K_i, which is the magnetic anisotropy constant of the ith region. The contribution of the ith region to the anisotropy constant of the whole sample is

$$K_i f_i = (b_i - b_{i+1}) H_i \tag{2}$$

and the volume fraction occupied by the ith region is

$$f_i = \frac{2}{\mu_0 M_s}\left(\frac{T_i - T_{i-1}}{H_i - H_{i-1}} - \frac{T_{i+1} - T_i}{H_{i+1} - H_i}\right), \tag{3}$$

where b_i is the slope of the uniaxial torque amplitude between the experimental points corresponding to the applied magnetic fields H_{i-1} and H_i, b_{i+1} is the slope corresponding to the applied magnetic fields between H_i and H_{i+1}, and M_s is the saturation magnetization of the material.

The magnetostatic effect due to the surface roughness was not studied because the samples were prepared in a vacuum and they do not present appreciable surface roughness.

The results of the model applied to the experimental torque data of $Fe_{80}B_{20}$ and $Co_{70}Mn_5Fe_1Mo_1Si_{14}B_9$ are presented in Tables I and II, respectively. The tables are divided in three blocks. The first block shows the estimated internal magnetic field and the corresponding magnetic anisotropy K_i of each region. In the second block, the results for the samples obtained without the applied magnetic field are presented. The first column shows the values of the uniaxial torque amplitude per unit volume T_u measured by means of the torque magnetometer. The second column shows the val-

TABLE II. Anisotropy distribution of $Co_{70}Si_{14}B_9Mn_5Fe_1Mo_1$ in the samples made with and without the applied magnetic field.

		Without the applied magnetic field			With the applied magnetic field		
$\mu_0 H$ (*T*)	K_i (Jm^{-3})	T_u (Jm^{-3})	$f_i(10^{-2})$	$f_i K_i$	T_u (Jm^{-3})	$f_i(10^{-2})$	$f_i K_i$
0.9974	317474	100	0.009	29.9	740	0.000	0.00
0.7974	253812	94	0.004	10.6	740	0.004	10.6
0.4974	158319	81	0.013	20.2	736	0.023	37.1
0.2474	78741	60	0.022	17.7	714	0.018	14.0
0.1574	50093	46	0.022	10.9	701	0.143	71.7
0.1174	37361	37	0.008	2.93	677	0.150	55.8
0.0774	24629	27	0.016	3.87	634	0.503	124
0.0374	11896	15	0.016	1.87	527	1.155	137
0.0174	5530	8	0.079	4.34	400	5.671	314
0.0074	2347	2	0.188	4.42	156	7.665	180

Downloaded 29 Dec 2004 to 193.144.85.71. Redistribution subject to AIP license or copyright, see http://jap.aip.org/jap/copyright.jsp

ues of the volume fraction $f_i(\%)$ of the zone in the sample affected by the magnetic anisotropy with the value K_i. The difference between the sum of the values of f_i and 100 is the volume fraction of the amorphous matrix. The last column contains the contribution of each zone to the total uniaxial torque amplitude measured in the torque magnetometer. This contribution is calculated as the product $f_i k_i$. Finally, the third block shows the results for the samples produced with the applied magnetic field.

Looking at Tables I and II, we can point out the following characteristics:

(a) The regions with a higher anisotropy in general occupy a smaller volume of fractions.
(b) For the samples made without the applied magnetic field, the highest anisotropies (above 10^5 Jm^{-3} in $Fe_{80}B_{20}$ and 5×10^4 Jm^{-3} in $Co_{70}Mn_5Fe_1Mo_1Si_{14}B_9$) contribute more than the low anisotropies to the total anisotropy. On the other hand, in the case of the samples made with the applied magnetic field, the lowest anisotropies (below 2.5×10^4 Jm^{-3} in both materials) have the highest contribution to the total anisotropy.

From the two tables, we can observe a great difference between the anisotropy distribution of the samples made with and without the applied magnetic field in both the materials.

For the $Fe_{80}B_{20}$ samples made without the applied magnetic field, the anisotropies up to 2.5×10^4 Jm^{-3} occupy only 0.4% of the volume, meanwhile, in those samples made with the applied magnetic field, these anisotropies occupy 9% of the volume. This change is more dramatic in $Co_{70}Mn_5Fe_1Mo_1Si_{14}B_9$ in which these anisotropies occupy 0.3% of the volume in the samples made without the applied magnetic field and 15% in those made with the applied magnetic field.

The mentioned results show that in the samples made with the applied magnetic field, the low anisotropies occupy a large volume and have a large contribution to the total anisotropy. Some regions present very high values of anisotropy constants ($>10^5$ Jm^{-3}). These regions are the zones with abrupt changes from the average characteristics of the amorphous phase that can remain unsaturated up to high magnetic fields. In our case with a demagnetizing factor of about 0.01 and with a saturation magnetization M_s between 4.5×10^5 and 8×10^5 Am^{-1}, the shape anisotropy for these amorphous ribbons would be about 10^5 Jm^{-3}. These demagnetizing factors can originate from elongated microholes, precipitates, and overstrained zones.

To compare the previously mentioned induced anisotropies with those induced by the static field annealing, we have performed a thermal treatment for 2 h with an applied magnetic field of 0.009 T, transverse to the longitudinal direction of the ribbon to the samples of both compositions made without the applied magnetic field. The torque curves for the two materials also show the twofold shape that corresponds to a uniaxial magnetic anisotropy. The easy axis is in the transverse direction of the ribbon (the direction of the applied magnetic field) in the two materials, and the induced anisotropies are 260 Jm^{-3} for $Fe_{80}B_{20}$ and 207 Jm^{-3} for $Co_{70}Mn_5Fe_1Mo_1Si_{14}B_9$.

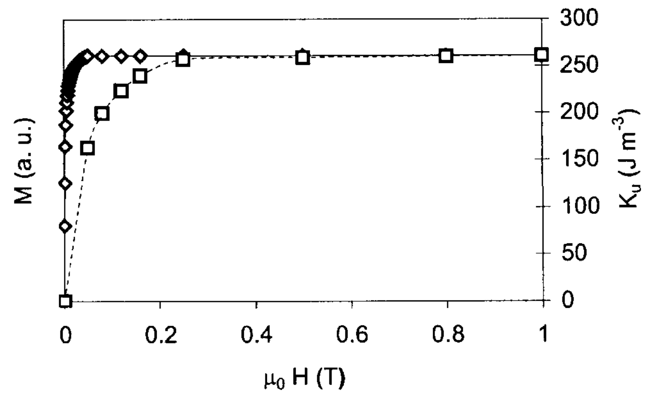

FIG. 4. Evolution of the magnetization (◇) and the magnetic anisotropy K_u (□) with the applied magnetic field for $Fe_{80}B_{20}$ after magnetic annealing. The dashed line corresponds to the magnetic anisotropy axis.

Figures 4 and 5 show the evolution of the magnetization and magnetic anisotropy constant with the applied magnetic field μ_0H for $Fe_{80}B_{20}$ and $Co_{70}Mn_5Fe_1Mo_1Si_{14}B_9$, respectively, after magnetic annealing. In order to apply the model developed by Tejedor *et al.*[14] in the present work, we have chosen the scales of both magnitudes, such that their saturation values coincide. As can be seen, the behavior of these curves can be summarized as follows:

(1) $Fe_{80}B_{20}$: K_u increases rapidly at low fields and practically saturates at 0.5 T. At this magnetic field, the magnetic anisotropy constant is 260 Jm^{-3}.
(2) $Co_{70}Mn_5Fe_1Mo_1Si_{14}B_9$: K_u increases slowly and at about 0.8 T, it reaches its maximum value of 207 Jm^{-3}.

We have applied the method indicated earlier to analyze the in-plane magnetic anisotropy induced by the static field annealing, and the results are shown in Tables III and IV. Looking at these tables, we can mention the following characteristics: (a) The regions with a higher anisotropy in general occupy a smaller volume of fractions and (b) the lowest anisotropies have the highest contribution to the total anisotropy due to their larger volume fraction.

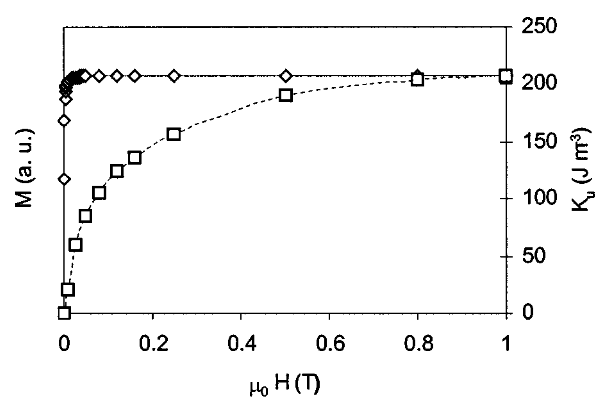

FIG. 5. Evolution of the magnetization (◇) and the magnetic anisotropy K_u (□) with the applied magnetic field for $Co_{70}Si_{14}B_9Mn_5Fe_1Mo_1$ after magnetic annealing. The dashed line corresponds to the magnetic anisotropy axis.

Downloaded 29 Dec 2004 to 193.144.85.71. Redistribution subject to AIP license or copyright, see http://jap.aip.org/jap/copyright.jsp

TABLE III. Anisotropy distribution of $Fe_{80}B_{20}$ in the samples annealed with the magnetic field.

		$Fe_{80}B_{20}$		
$\mu_0 H$ (T)	K_i (Jm^{-3})	T_u (Jm^{-3})	$f_i(10^{-2})$	$f_i K_i$
0.9947	633275	261	0.001	4.97
0.7947	505951	260	0.001	1.32
0.4947	314965	258	0.004	12.5
0.2447	155810	250	0.011	16.6
0.1447	92148	240	0.063	49.2
0.0947	60317	218	0.025	15.2
0.0647	41218	200	0.149	55.0
0.0447	28486	171	0.373	106
0.0347	22120	135	0.045	9.92
0.0117	7477	80	0.694	51.9

In the case of the magnetic-annealed ribbons of $Fe_{80}B_{20}$ and $Co_{70}Si_{14}B_9Mn_5Fe_1Mo_1$, the tendency of the results observed in Tables III and IV indicates that the volume of fractions that correspond to the anisotropies up to 2.5×10^5 Jm^{-3} is three times greater than in the case of the as-quenched samples made without the applied magnetic field.

If we compare the results obtained for the samples made with an applied magnetic field with those obtained for the static magnetic-annealed samples, it can be pointed out that, apart from the fact that the induced transverse magnetic anisotropies are greater in the samples made with the applied magnetic field, the dependence of T_u on the applied magnetic field are very similar, in both kinds of samples, the lowest anisotropy regions have the highest contribution to the total anisotropy.

TABLE IV. Anisotropy distribution of $Co_{70}Si_{14}B_9Mn_5Fe_1Mo_1$ in the samples annealed with the magnetic field.

		$Co_{70}Si_{14}B_9Mn_5Fe_1Mo_1$		
$\mu_0 H$ (T)	K_i (Jm^{-3})	T_u (Jm^{-3})	$f_i(10^{-2})$	$f_i K_i$
0.9974	317474	207	0.005	15.0
0.7974	253812	204	0.010	25.2
0.4974	158319	190	0.031	48.4
0.2474	78741	154	0.018	13.8
0.1474	46910	134	0.038	17.7
0.0974	30995	118	0.025	7.79
0.0674	21445	106	0.110	23.6
0.0474	15079	91	0.368	55.5
0.0224	7121	60	0.453	32.3
0.0074	2347	20	0.014	0.34

Finally, the samples made with the applied magnetic field were submitted to a thermal treatment, above the Curie temperature. After the thermal treatment, the anisotropy constant for $Fe_{80}B_{20}$ fell to 247 Jm^{-3} and the easy axes is now at 9° from the transverse direction. For $Co_{70}Si_{14}B_9Mn_5Fe_1Mo_1$, the anisotropy was reduced from 740 to 310 Jm^{-3} with the easy axis at 40° from the transverse direction of the ribbon.

Taking into account the similarities between the results in the static magnetic annealing and those on the samples made with an applied magnetic field, it looks like that the mechanism of the inducing magnetic anisotropy by applying a magnetic field during the solidification process in the amorphous ribbons is the same as the one that produces magnetic anisotropy by the static magnetic annealing.

In conclusion, we have analyzed the magnetic anisotropy induced in the amorphous magnetic ribbons by applying a magnetic field during the solidification of the melt in the quenching process. The different sources of this induced in-plane magnetic anisotropy have been discriminated using a model based on the study of the evolution of the magnetization and the uniaxial torque with the applied magnetic field.

ACKNOWLEDGMENT

This work was supported in part by the MCyT, Madrid, Spain, under Grant No. MAT 2000-0623.

[1] M. Takahashi and S. Ishio, Jpn. J. Appl. Phys. **29**, 129 (1979).
[2] H. N. Ok and A. H. Morrish, Phys. Rev. B **23**, 2257 (1981).
[3] M. Tejedor, J. A. García, and J. Carrizo, J. Magn. Magn. Mater. **131**, 329 (1994).
[4] J. D. Livingston, W. G. Morris, and T. Jagielinsky, IEEE Trans. Magn. **19**, 1916 (1983).
[5] P. Allia, F. E. Luborsky, G. P. Soardo, and F. Vinai, J. Appl. Phys. **52**, 3553 (1981).
[6] B. S. Berry and W. C. Pritchet, Phys. Rev. Lett. **34**, 1022 (1975).
[7] J. M. Barandiarán, A. García-Arribas, and J. Gutierrez, J. Magn. Magn. Mater. **133**, 46 (1994).
[8] M. Tejedor, J. A. García, J. Carrizo, L. Elbaile, and J. D. Santos, Appl. Phys. Lett. **82**, 937 (2003).
[9] M. Tejedor, J. A. García, J. Carrizo, L. Elbaile, J. D. Santos, J. Mira, and J. Rivas, J. Appl. Phys. **86**, 2185 (1999).
[10] M. Tejedor, J. A. García, and J. Carrizo, J. Phys. E **22**, 362 (1989).
[11] M. Tejedor, J. A. García, and J. Carrizo, J. Magn. Magn. Mater. **117**, 141 (1992).
[12] L. P. Tarasov, Phys. Rev. **56**, 1224 (1939).
[13] J. S. Kouvel and C. D. Graham, Jr., J. Appl. Phys. **28**, 340 (1957).
[14] M. Tejedor, J. A. García, and J. Carrizo, J. Magn. Magn. Mater. **118**, 333 (1993).

Downloaded 29 Dec 2004 to 193.144.85.71. Redistribution subject to AIP license or copyright, see http://jap.aip.org/jap/copyright.jsp